JOURNAL OF PROPULSION AND POWER
Vol. 17, No. 1, January–February 2001

Effect of Reynolds Number on Separation Bubbles on Compressor Blades in Cascade

Garth V. Hobson,* Denis J. Hansen,† David G. Schnorenberg,† and Darren V. Grove†
Naval Postgraduate School, Monterey, California 93943-5000

A detailed experimental investigation of second-generation, controlled-diffusion, compressor stator blades at an off-design inlet-flow angle was performed in a low-speed-cascade wind tunnel primarily using laser Doppler velocimetry (LDV). The object was to characterize the flowfield in the Reynolds number range of 2.1–6.4 × 10^5 and to obtain LDV measurements of the suction surface boundary-layer separation that occurred near midchord. Surface flow visualization showed that at the low Reynolds number the midchord separation bubble started laminar and reattached turbulent within 20% chord on the suction side of the blade. The extent of the bubble compared very well with the measured blade surface pressure distribution, which showed a classical plateau and then diffusion in the turbulent region. LDV measurements of the flow reversal in the bubble were performed. At the intermediate Reynolds number, the boundary layer was transitional upstream of the separation bubble that had decreased significantly in size (down to 10% chord). At the highest Reynolds number, the flow was turbulent from close to the leading edge, and three-dimensional flow reversal as a result of endwall effects appeared at approximately 80% chord. These data, particularly the low Reynolds number data, are an excellent test case for either large-eddy simulation or direct numerical simulation of cascade flowfields.

Nomenclature

C	=	chord length, mm
Cp	=	coefficient of pressure, $(p - p_\infty)/\frac{1}{2}\rho W_{\text{ref}}^2$
d	=	normal distance from the blade, mm, or fringe spacing, μm
H	=	shape factor
L	=	focal length, mm
P	=	atmospheric or plenum pressures, Pa
p	=	pressure, Pa
S	=	blade pitch, or spacing, mm
T	=	temperature, K
U	=	axial velocity, m/s
u'	=	axial velocity turbulent fluctuation, m/s
V	=	tangential velocity, m/s
v'	=	tangential velocity turbulent fluctuation, m/s
W	=	total velocity, $\sqrt{(U^2 + V^2)}$, m/s
X	=	distance from the blade, mm
x	=	axial direction; also vertical direction in the cascade, mm
Y	=	distance from the blade, mm
y	=	tangential direction; also horizontal direction, mm
β	=	flow angle, measured from the axial, deg
δ	=	displacement thickness, mm
η	=	normal to the chordwise direction, mm
θ	=	momentum thickness, mm
κ	=	beam half-angle
λ	=	wavelength of laser light, nm
ξ	=	chordwise direction, mm
ρ	=	density, kg/m^3
ω	=	mass-averaged total pressure loss coefficient

Subscripts

atm	=	atmospheric conditions
f	=	fringe spacing
ref	=	upstream reference conditions
t	=	plenum conditions
0	=	stagnation conditions
1	=	upstream, or lower, traverse slot
2	=	downstream, or upper, traverse slot

Received 24 June 1999; revision received 18 April 2000; accepted for publication 19 April 2000.

*Associate Professor, Department of Aeronautics and Astronautics, Turbopropulsion Laboratory.

†Graduate Student, Department of Aeronautics and Astronautics, Turbopropulsion Laboratory.

Introduction

AS stated in Ref. 1 (page 45), "At high flight altitudes and low flight speeds, the Reynolds number of the flow through the inlet stages of a compressor becomes so low that their performance is often impaired." The present study used a set of second-generation controlled-diffusion (CD) stator blades in cascade to study the effect of Reynolds number that would be experienced with such flight condition changes. The blades were designed as stator 67B and tested as stage 67B by Gelder et al.[2] with stage 67 being one of the transonic compressor stages that NASA has tested.[3] The design-point Reynolds number, based on chord, for stator 67B was almost one million at sea level, and this was estimated to decrease to 2×10^5 at 1.5×10^4 m. Three Reynolds numbers, namely, 6.4×10^5, 3.8×10^5, and 2.1×10^5, were tested with 10 stator 67B blades in cascade in the Naval Postgraduate School (NPS), Low-Speed Cascade Wind Tunnel. Many earlier cascade wind-tunnel tests have been conducted to study the effect of Reynolds number on blade element performance, most notably by Rhoden,[4] Horlock et al.,[5] Schlichting and Das,[6] Evans,[7] and Roberts.[8] The last three works were also concerned with the effects of freestream turbulence, which is also important to blade performance. All of these two-dimensional cascade tests indicated a deterioration in performance when the Reynolds number was decreased below 1×10^5; however, most of the earlier tests were conducted at Reynolds numbers well below 5×10^5 (Ref. 1).

The present study has four motivating points. First, the Reynolds number range that the cascade (and blade chord of 12.7 cm) could produce is more representative of flight conditions. Second, the blade profiles were the midsection of a modern design that had been rig tested.[2] Third, the present study is seen as a challenging test case for turbulence and transition models used in numerical prediction of separated flows. Finally, these data, particularly the low Reynolds number data, are an excellent test case for either large-eddy simulation or direct numerical simulation of cascade flowfields.

Sanger[9] designed stator 67A with CD blade profiles to replace the original double-circular-arc profiles of stage 67. The object of the study was to implement a design optimization procedure in replacing

the original blades with the same blade count. These blade profiles were extensively tested in the NPS cascade wind tunnel.[10,11] The subsequent design and testing of stator 67B by Gelder et al.[2] was to improve on the performance of the stator 67A blade row by halving the blade count while still performing the same amount of flow turning. The blades of stator 67B were more highly loaded than those of stator 67A and, thus, are more cambered; however, the leading edge shapes of 67B were made elliptic (as opposed to the circular leading edge of 67A) in an attempt to eliminate leading-edge separation that was prevalent on stator 67A.

Experimental Apparatus and Procedure

The Low-Speed Cascade Wind Tunnel of the NPS Turbopropulsion Laboratory was used throughout this study. The inlet flow uniformity and periodicity had been thoroughly documented by Elazar,[10] with 20 stator 67A blades in the cascade. A schematic of the cascade is shown in Fig. 1. In the test section, 10 stator 67B profiles were installed.

Each blade had an aspect ratio of 1.996, and the solidity of the blade row was 0.835. Figure 2 shows the blade profile, and the machine coordinates are given in the Appendix. Table 1 contains a summary listing of the geometrical parameters of the cascade test section. A two-component laser-Doppler velocimeter was used for the laser Doppler velocimetry (LDV) measurements at the station locations denoted in Fig. 3. The velocity components measured were the vertical, U, or axial velocity and the horizontal, V, or tangential velocity, and all of the measurements were taken in the coincidence mode. For the seed material, 1-μm oil mist particles were used. These were introduced into the flow at the location shown in Fig. 1. All measurements recorded were for 1000 data points at a typical data rate of 200 particles per second, and no editing was used to present the data. Suitable tilting and yawing of the LDV was performed to allow access as close to the blade surfaces as possible, particularly during the boundary-layer surveys, as shown in Fig. 3. All boundary-layer surveys were performed over a distance of 14% of the blade chord in a direction normal to the blade surface.

Loss measurements were performed with a traversing five-hole probe at the upper traverse slot (Fig. 1) for the near-design inlet flow angle test case. Flow unsteadiness due to trailing-edge separation precluded these measurements at the increased incidence. Blade surface pressure measurements were recorded from an instrumented blade that had 48 pressure ports machined into its surface. Surface flow visualization was performed with a titanium dioxide and kerosene mixture. Both video of the developing surface flow patterns and still photography of the end result once the mixture had dried on the blade surfaces were recorded.

The estimated measurement uncertainties are given in Table 2. The uncertainties in parameters κ, L, and λ were given by the manufacturer. The fringe spacing was calculated as $d_f = \lambda/\sin\kappa$.

Table 1 Test section specifications

Property	Value
Blade type	Stator 67B CD
Number of blades	10
Blade spacing	152.40 mm
Chord	127.14 mm
Setting angle	16.3 deg ± 0.1 deg
Span	254.0 mm

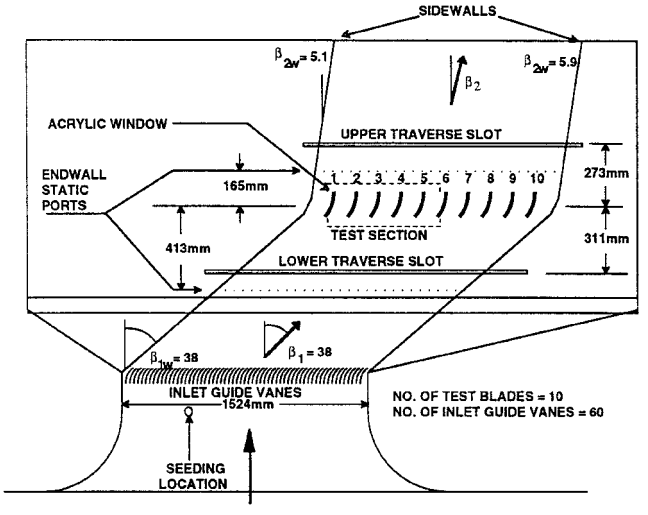

Fig. 1 Low-speed cascade wind-tunnel schematic.

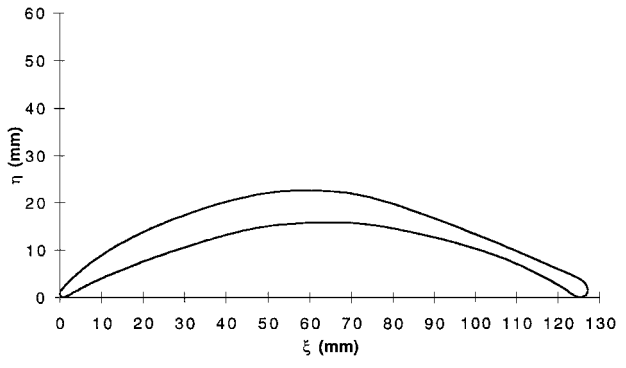

Fig. 2 Blade profile.

Table 2 Estimated measurement uncertainty

Item	Description	Uncertainty
X, Y	Distance from blade surface	0.025 mm
P_t	Plenum pressure	25 Pa
p	Pressure	12 Pa
P_{atm}	Atmospheric pressure	35 Pa
T_t	Plenum temperature	0.2°C
——	LDV clock counter	1 n-s
κ	Beam half angle	0.3 deg
L	Focal length	7.6 mm
λ	Wavelength	0.1%
d_f	Fringe spacing	0.3%
U, V	Particle velocity	
	at 10 m/s	0.33%
	at 100 m/s	0.65%

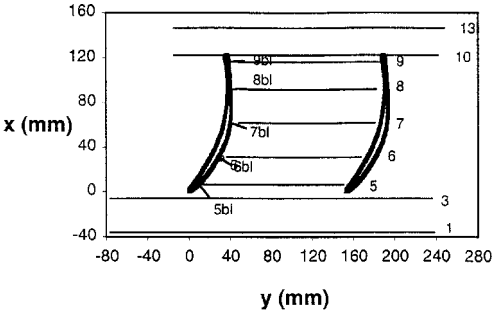

Fig. 3 Pitchwise and boundary layer survey locations with station designations.

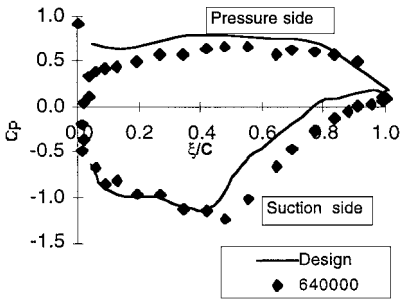

Fig. 4 Blade surface pressure distribution at 36-deg inlet flow angle.

Because particles do not follow the flow exactly, the uncertainty in the velocity can be larger than the uncertainty in the particle velocity.

Results and Discussion

Blade Surface Pressure Distributions

Measurements were performed on the cascade at the high Reynolds number of 6.4×10^5 by Hansen[12] at the near-design inlet flow angle of 36 deg. Figure 4 shows the results of the blade surface pressure distribution measurements in terms of the coefficient of pressure Cp plotted along the blade chord at various positions given by the ratio ξ/C. The Gelder et al. design[2] intent for stator 67B is shown plotted with the solid black line. The discrepancy between the two sets of measurements show that three-dimensional effects dominated in the compressor measurements vs the nearly two-dimensional flow in the cascade. Five-hole probe surveys upstream and downstream of the blade row yielded an ax-

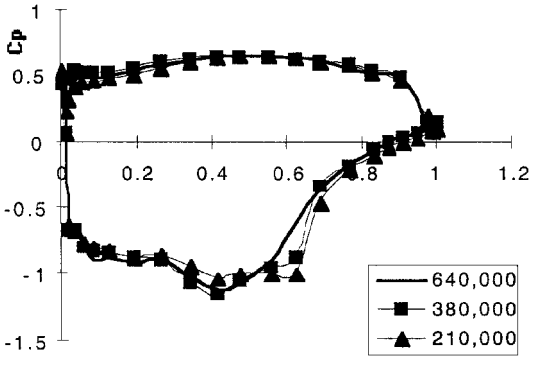

Fig. 5 Blade surface pressure distribution at 38-deg inlet flow angle.

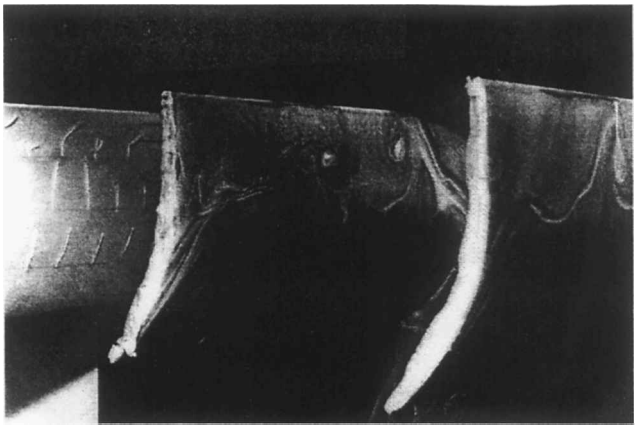

Fig. 6 Surface flow visualization at 6.4×10^5 Reynolds number and 38-deg inlet flow angle.

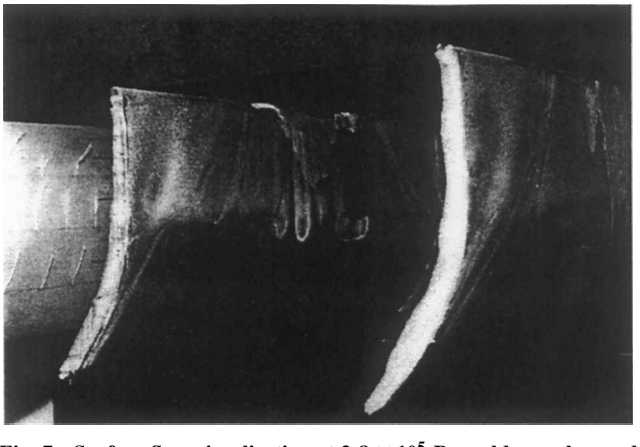

Fig. 7 Surface flow visualization at 3.8×10^5 Reynolds number and 38-deg inlet flow angle.

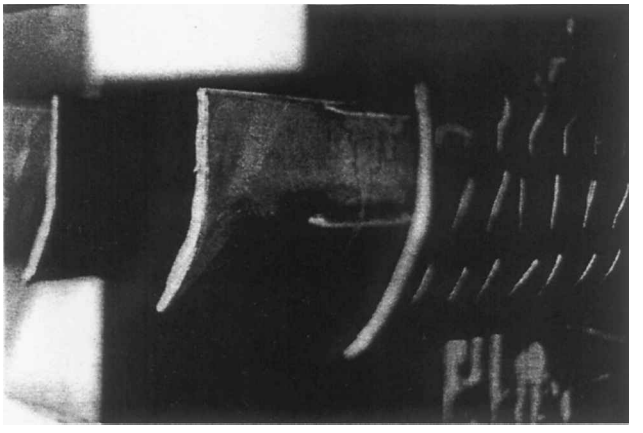

Fig. 8 Surface flow visualization at 2.1×10^5 Reynolds number and 38-deg inlet flow angle.

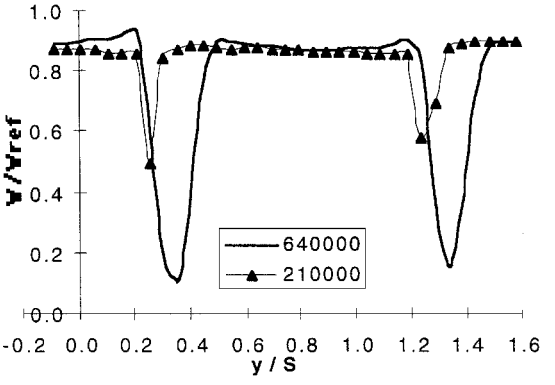

Fig. 9 Wake profiles at 38-deg inlet flow angle for the highest and lowest Reynolds number flows.

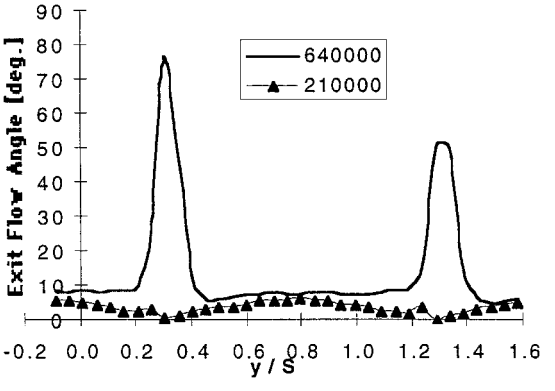

Fig. 10 Exit flow angle distributions for the highest and lowest Reynolds number flows.

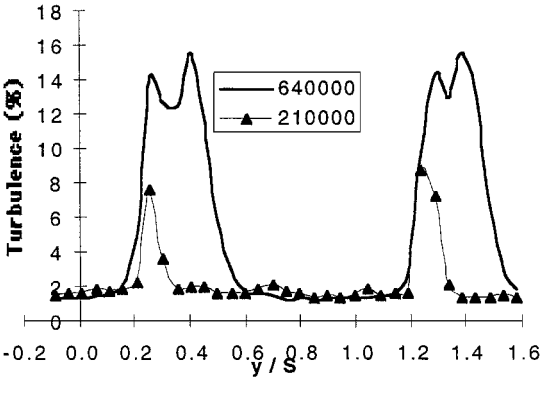

Fig. 11 Exit turbulence distributions for the highest and lowest Reynolds number flows.

ial velocity density ratio (AVDR) ($=\overline{\rho_2 U_2}/\overline{\rho_1 U_1}$, where the overbar represents mass averaged quantities) of 1.03 and the loss coefficient, $\omega = (\bar{p}_{02} - \bar{p}_{01})/(\bar{p}_{01} - \bar{p}_1)$, was 0.030. The experimentally determined loss coefficient[2] of the stator blade element at 50% span in stage 67B was 0.029.

The *Cp* distribution at the three Reynolds numbers are shown in Fig. 5. All of these measurements were performed at an inlet flow angle $\beta = 38$ deg (Ref. 13). The distribution on the suction side of the blade for the high Reynolds number rose continuously from the minimum pressure location at 40% chord and, thus, showed no indication of flow separation. The distribution at the intermediate Reynolds number of 3.8×10^5 implied a separation region between approximately 50 and 65% chord. At the low Reynolds number (2.1×10^5), the distribution implied a separation region between 45 and 70% chord because of the plateau in the midchord region of the suction surface. The separation region had moved forward with decreasing Reynolds number, and the separation bubble had also affected the minimum suction peak by reducing its magnitude. Both of these observations are consistent with earlier separation bubble studies.[4,5,8]

Flow Visualization

Surface flow visualization was performed on blades 3 and 4 in the cascade at the three Reynolds numbers. The flow pattern at the high Reynolds number (Fig. 6) revealed that the flow was three dimensional in the trailing-edge region due to the formation of

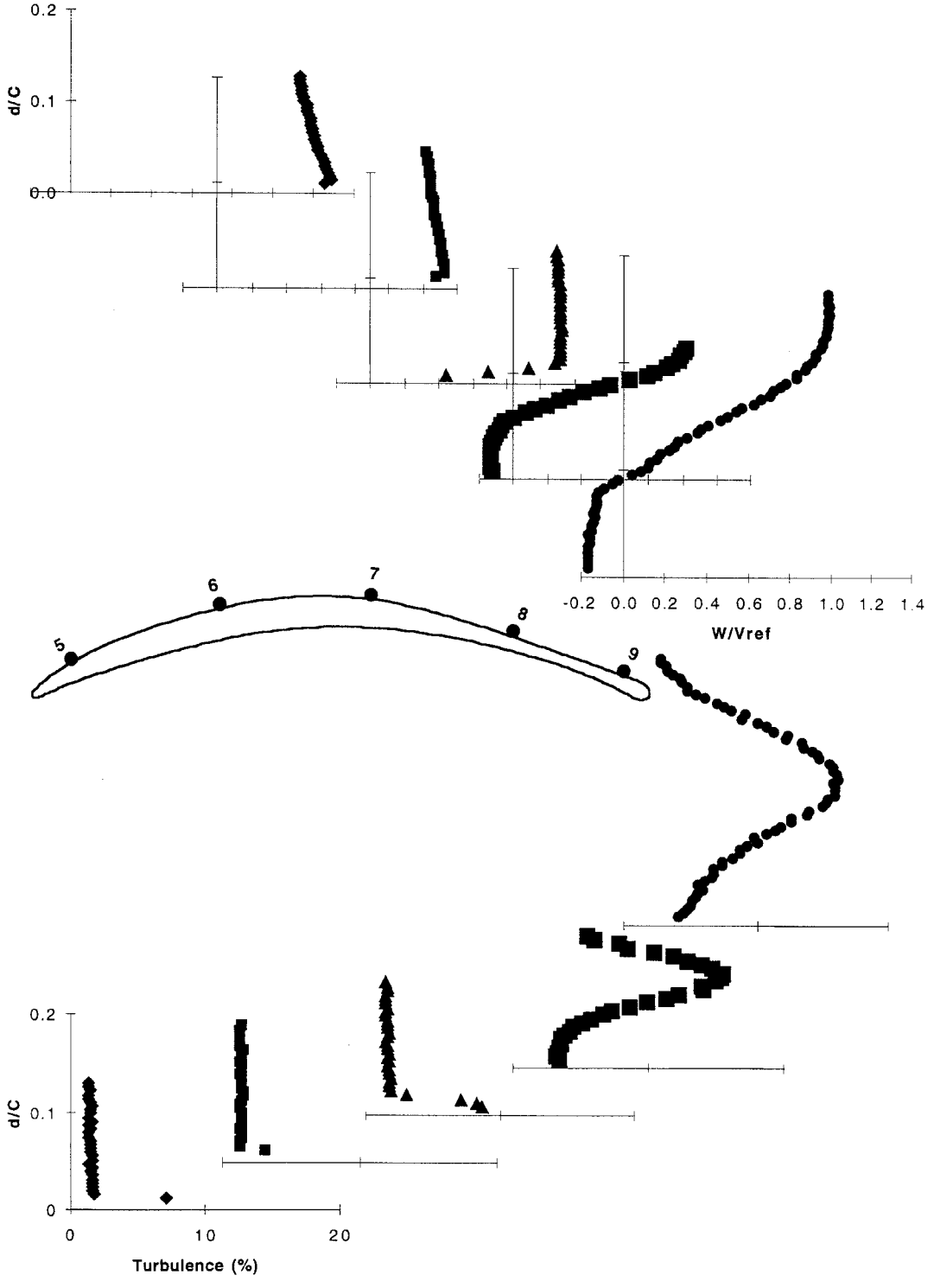

Fig. 12 Suction-surface boundary-layer profiles at 6.4×10^5 Reynolds number.

corner vortices in the vicinity of the cascade endwalls. In addition, the flow was not symmetric about the midspan due to the different boundary-layer thicknesses between the two endwalls, which resulted in different vortex locations on the blade surface. The flow visualization at the intermediate Reynolds number (Fig. 7) indicated two-dimensional flow along most of the midspan section as well as good periodicity between the blades. A region of spanwise intermittent separation was noted and measured at a position corresponding to 46% chord with a reattachment point at 57% chord. Intermittent separation means that where the boundary layer had undergone transition to turbulent flow, either naturally or due to local surface roughness, separation had not yet occurred. This gave rise to the regions where no TiO_2 was present, that is, the vertical black streaks on the blade at midspan. In the regions along the span of the blade where transition of the boundary layer was suppressed, then laminar separation occurred, as was noted by the spanwise intermittent separation bubbles. The actual separation point (without the surface fluid) was closer to the trailing edge because gravitational effects had moved the fluid in the separation bubble downward toward the leading edges. The measured separation region correlated well with the Cp distribution that indicated a separation region between approximately 50 and 65% chord. The flow visualization at the low Reynolds number (Fig. 8) indicated two-dimensional flow along most of the midspan section. A region of laminar separation was noted and measured at a position corresponding to 39% chord with a reattachment point at approximately 63% chord. A small amount of TiO_2/kerosene fluid was suspended in this region. Again taking into account the gravitational effects on the suspended fluid, the measured separation region correlated well with the Cp distribution, which indicated a separation region between approximately 45 and 70% chord.

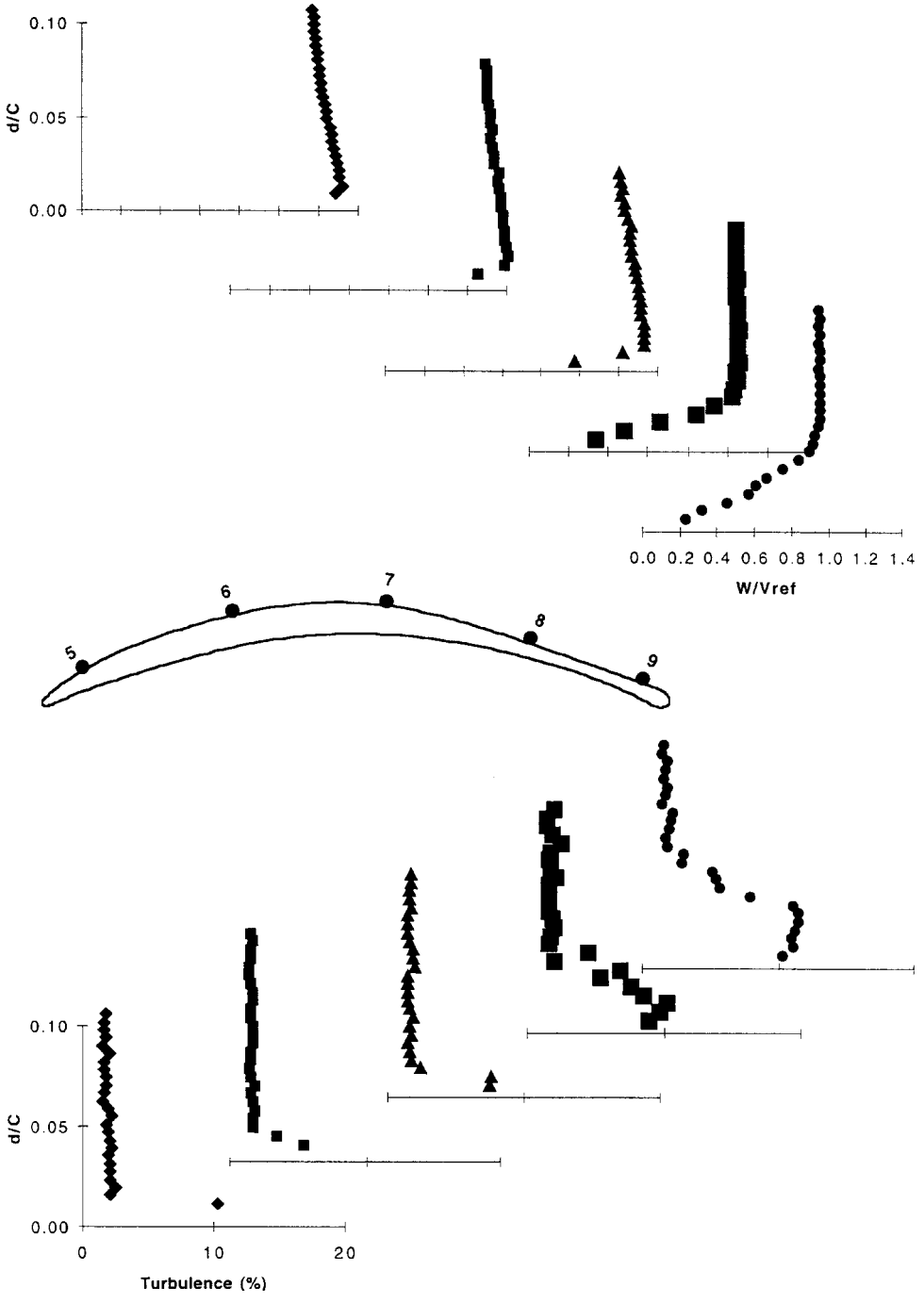

Fig. 13 Suction-surface boundary-layer profiles at 3.8×10^5 Reynolds number.

Inlet and Wake Profiles

Inlet flowfield surveys were conducted at station 1, 30% of an axial chord ahead of the blade leading edges, over two blade pitches. The summarized inlet flow conditions are presented in Table 3. The total velocity was uniform to within 1% for all of the tests, and because the survey points were equispaced, the average values tabulated can also be considered as mass-averaged values.

The average inlet flow angle increased by 0.6 deg when reducing the Reynolds number from the high to the low value, as did the potential effect of the blades on the incoming flow due to the increased pitchwise flow angle variation (or standard deviation). At the high Reynolds number, the inlet turbulence was almost 1.6%, which was consistent with earlier measurements on the first set of CD blades.[10,11] However for the low Reynolds number flow case, the turbulence had increased by almost 20% to about 1.9%. The definition of turbulence is

$$\text{turbulence} = \tfrac{1}{2}\sqrt{(\bar{u}')^2 + (\bar{v}')^2}\Big/ W_{\text{ref}} \tag{1}$$

Table 3 Inlet flow conditions

Reynolds number, $\times 10^5$	Average inlet flow angle, deg	Inlet flow angle standard deviation	Average inlet turbulence, %	Inlet turbulence standard deviation
6.4	37.7	1.21	1.6	0.15
3.8	38.2	1.37	1.6	0.14
2.1	38.3	1.48	1.9	0.27

The wake total velocity profiles are shown in Fig. 9 for only the highest and lowest Reynolds number flows. These were measured at station 13, which was 20% of an axial chord downstream of the trailing edges.

First, periodicity is evident in both profiles; second, the significantly larger wake width and deficit for the high Reynolds number case are evident. At this station, the minimum velocity was only

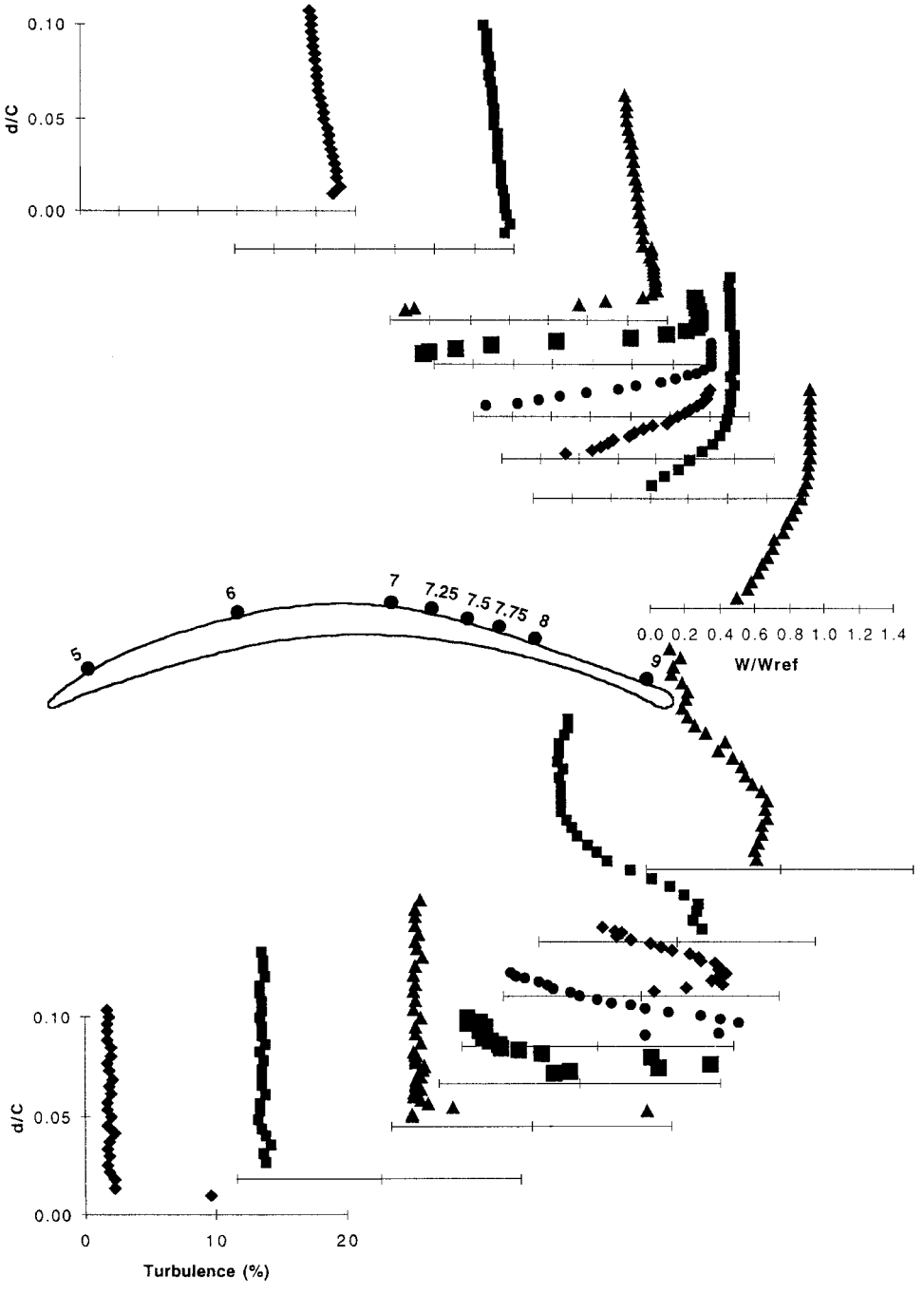

Fig. 14 Suction-surface boundary-layer profiles at 2.1×10^5 Reynolds number.

10% of the core flow. At preceding stations, reverse flow was measured, which indicated that the trailing edge had separated. The individual velocity components for the wake distributions for all three Reynolds numbers were presented by Schnorenberg.[13]

The exit flow angle distributions for the high and low Reynolds number cases were also significantly different, as shown in Fig. 10. At the high Reynolds number, the mass-averaged exit flow angle was 9.25 deg, and this value decreased with decreasing Reynolds number to 4.56 and 3.74 deg, respectively, for Reynolds numbers of 3.8×10^5 and 2.1×10^5. At the 6.4×10^5 Reynolds number, the peak flow angle in the wake was in excess of 50 deg, and the flow angle distribution between the blades was relatively uniform; whereas for the 2.1×10^5 Reynolds number, the flow angle in the core flow showed a maximum halfway between the blades. This profile was similar to the design exit flow angle distribution measured by Hansen[12] at the high Reynolds number.

The exit turbulence distributions are shown in Fig. 11, where the profile for the separated boundary layer showed the double-peaked distribution. Each peak corresponded to the maximum velocity gradient shown in Fig. 9. The resolution of the measurements for the low Reynolds number test case were not sufficient to resolve the aforementioned double-peak distribution.

Good periodicity was evident in the turbulence profiles when compared to the exit flow angle distributions in Fig. 10. The freestream turbulence was measured to be approximately 1.4% for all three Reynolds numbers, although the inlet turbulence was inversely proportional to Reynolds number as shown in Table 3.

Suction Surface Boundary Layers

Total velocity and turbulence distributions are presented in Figs. 12 and 13 at stations 5–9 for the high and intermediate Reynolds numbers. At the high Reynolds number, reverse flow was measured at stations 8 and 9 with corresponding increased turbulence levels. As seen in the flow visualization (Fig. 6), the flow over the suction surface was three dimensional and so these two-component measurements need to be interpreted accordingly.

No reverse flow was measured at the intermediate Reynolds number (Fig. 13). This could be due to the spanwise variation of axial transition location on the suction surface. When boundary-layer transition occurred, flow separation was suppressed (Fig. 7). The LDV measurements were taken over a region where transition had occurred, as is evident by the increase of turbulence in the boundary layer at stations 5–7. The blade surface pressure measurements, which showed a separation bubble plateau for the intermediate Reynolds number, were taken on blade 6 (Fig. 1), and all of the LDV measurements were performed between blades 3 and 4. Another explanation for discrepant LDV and pressure measurements could be the spanwise variation of the separation bubbles at the transitional Reynolds number of 3.8×10^5.

At the lowest Reynolds number (Fig. 14), reverse flow was measured at station 7.25 (25% axial distance between stations 7 and 8) at the first two points away from the blade surface. As can be seen from the upstream profiles, the boundary layers were laminar because of the reduced turbulence levels.

By station 7.75, the profile exhibited the character of a reattached turbulent boundary layer, with increased growth rate and increased turbulence levels. At the last two stations (8 and 9), the turbulence profile exhibited a double-peaked distribution. The outer peak is due to the free shear layer over the bubble, and inner peak is due to the reformation of the attached boundary layer. When comparing the relative size of the boundary layers between the high Reynolds number case and the low Reynolds number case, it can be seen that the separated boundary profile (Fig. 12, station 9) is larger than the attached profile (Fig. 14). In Fig. 15, the displacement thickness for the high Reynolds number case is an order of magnitude larger at the trailing edge than the low Reynolds number test case. For both of the separated flow regions, at high and low Reynolds numbers, there is a localized increase in displacement thickness and shape factor

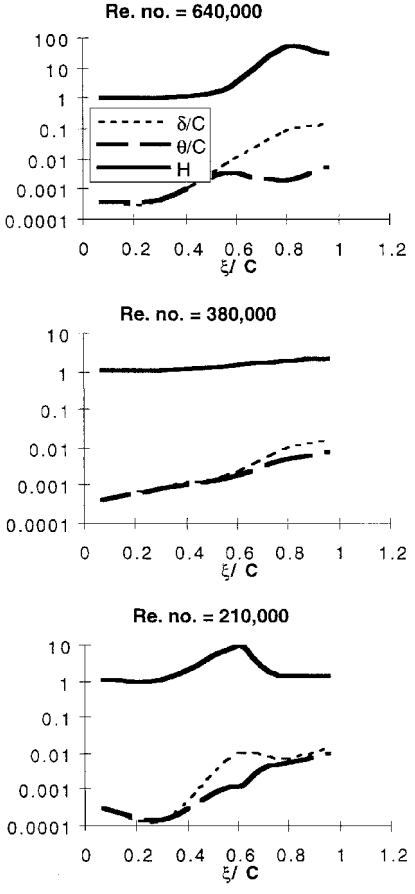

Fig. 15 Suction surface integral parameters of displacement thickness, momentum thickness, and shape factor for the three Reynolds numbers.

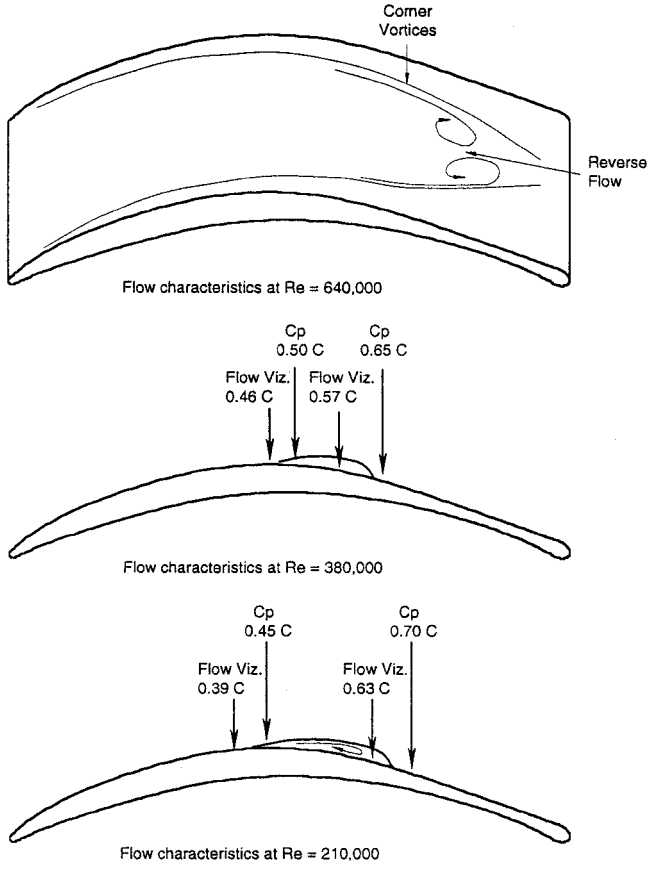

Fig. 16 Flow structure variation with Reynolds number.

with a leveling off of the momentum thickness. At the intermediate Reynolds number, the integral parameters increase continually along the suction surface.

Summary

Figure 16 shows the approximate flow structure for the three Reynolds numbers. The experimentally determined separation and reattachment locations for the low and intermediate Reynolds number cases are indicated. The region of flow reversal determined from flow visualization and LDV measured separation for the high Reynolds number case are also shown with the vortex structure on the blade surface. The three measurement techniques (flow visualization, surface pressure measurements, and LDV) all agree reasonably well, giving confidence in the proposed flow structure. Although the coarseness of the location of the LDV surveys precludes determining the separation point exactly, reverse flow measurements were obtained at the location between separation and reattachment for the low Reynolds number test case. For the two low Reynolds number cases, the separation points indicated by the flow visualization were consistently closer to the leading edge as a result of the effects of gravity on the TiO_2 mixture.

Conclusions

Detailed laser Doppler anemometry measurements of the flow over the suction surface of a set of second-generation CD compressor stator blades showed that as the Reynolds number was decreased from the design value of approximately 6.4 to 2.1×10^5 a laminar separation bubble, which reattached as turbulent, formed at midchord. The flow also became more two dimensional as the effect of the corner vortices were diminished as the Reynolds number was decreased. At the high Reynolds number, the trailing edge experienced turbulent flow reversal as a result of the interaction of the corner vortices. At the intermediate Reynolds number of 3.8×10^5, separation occurred on the suction surface when the approaching boundary layer remained laminar; however, when the boundary underwent transition to turbulent flow, then separation was suppressed, which gave rise to a spanwise variation of the separation bubble.

Additional pressure measurements and surface flow visualization confirmed the results obtained quantitatively with the LDV. These data should form a challenging test case for viscous flow calculations, particularly for the calibration of turbulence models and their ability to predict the effect of Reynolds number on the state of a boundary layer.

Appendix: Machine Coordinates

Table A1 Blade coordinates, mm (Fig. 2)

ξ	η	ξ	η	ξ	η	ξ	η	ξ	η	ξ	η
−0.02	0.74	42.22	20.63	114.06	8.20	126.77	0.60	98.46	10.69	27.66	9.83
−0.01	0.82	43.53	20.90	114.88	7.89	126.69	0.53	97.21	11.03	26.44	9.46
−0.01	0.90	44.84	21.16	115.69	7.58	126.60	0.45	95.97	11.37	25.21	9.09
0.01	0.97	46.14	21.40	116.51	7.27	126.48	0.38	94.72	11.69	24.01	8.71
0.03	1.05	47.48	21.62	117.32	6.97	126.38	0.32	93.48	12.00	22.80	8.34
0.06	1.13	48.81	21.82	118.14	6.66	126.30	0.28	92.23	12.30	21.59	7.95
0.09	1.20	50.14	22.00	118.95	6.36	126.22	0.25	90.97	12.58	20.38	7.56
0.13	1.28	51.48	22.16	119.57	6.13	126.15	0.22	89.72	12.86	19.18	7.16
0.17	1.35	52.81	22.29	120.18	5.90	125.99	0.17	88.46	13.11	17.97	6.76
0.22	1.43	54.14	22.40	120.80	5.68	125.77	0.12	87.20	13.36	16.97	6.42
0.28	1.51	55.49	22.49	121.41	5.45	125.31	0.08	85.95	13.60	15.98	6.08
0.35	1.58	56.84	22.55	122.03	5.22	125.08	0.09	84.69	13.83	14.98	5.73
0.42	1.66	58.18	22.59	122.64	4.98	124.93	0.11	83.44	14.05	13.98	5.37
0.75	1.98	59.53	22.60	123.04	4.82	124.70	0.14	82.18	14.26	12.99	5.02
1.07	2.29	60.88	22.59	123.45	4.65	124.55	0.18	80.92	14.46	11.99	4.65
1.40	2.60	62.22	22.56	123.85	4.49	124.39	0.22	79.66	14.65	11.21	4.36
1.72	2.89	63.57	22.50	124.25	4.32	124.24	0.27	78.41	14.83	10.42	4.07
2.04	3.19	64.91	22.42	124.65	4.14	124.09	0.32	77.15	15.00	9.64	3.77
2.37	3.47	66.25	22.31	125.05	3.96	124.01	0.35	75.90	15.15	8.86	3.47
2.90	3.91	67.59	22.18	125.23	3.88	123.94	0.38	74.64	15.28	8.07	3.16
3.42	4.34	68.93	22.03	125.38	3.80	123.86	0.41	73.39	15.41	7.29	2.83
3.95	4.76	70.27	21.85	125.52	3.73	123.78	0.45	72.14	15.51	6.71	2.59
4.47	5.16	71.58	21.65	125.65	3.65	123.71	0.48	70.88	15.60	6.12	2.33
5.00	5.55	72.88	21.42	125.77	3.58	123.63	0.52	69.63	15.67	5.54	2.07
5.53	5.93	74.19	21.17	125.88	3.50	123.56	0.56	68.38	15.73	4.96	1.81
6.28	6.46	75.50	20.90	125.98	3.42	123.48	0.60	67.13	15.77	4.37	1.54
7.03	6.97	76.81	20.61	126.08	3.35	123.39	0.66	65.88	15.80	3.79	1.27
7.78	7.46	78.12	20.29	126.17	3.27	123.03	0.90	64.64	15.81	3.41	1.09
8.53	7.93	79.39	19.97	126.26	3.20	122.66	1.13	63.39	15.81	3.02	0.91
9.28	8.39	80.67	19.64	126.34	3.12	122.30	1.35	62.14	15.79	2.64	0.72
10.03	8.83	81.94	19.29	126.41	3.04	121.94	1.57	60.90	15.77	2.26	0.54
11.01	9.39	83.21	18.93	126.48	2.97	121.58	1.78	59.66	15.73	1.87	0.35
11.99	9.92	84.49	18.56	126.55	2.89	121.21	1.99	58.42	15.69	1.49	0.17
12.97	10.42	85.76	18.18	126.61	2.81	120.64	2.30	57.18	15.63	1.42	0.13
13.95	10.91	87.01	17.80	126.67	2.74	120.07	2.59	55.94	15.55	1.34	0.10
14.93	11.39	88.26	17.41	126.72	2.66	119.51	2.88	54.70	15.46	1.27	0.07
15.91	11.84	89.50	17.01	126.77	2.59	118.94	3.16	53.47	15.35	1.19	0.05
17.12	12.40	90.75	16.61	126.82	2.51	118.37	3.43	52.24	15.23	1.12	0.03
18.34	12.93	92.00	16.19	126.86	2.43	117.80	3.70	51.00	15.09	1.04	0.01
19.55	13.45	93.25	15.77	126.90	2.36	117.02	4.07	49.77	14.93	0.96	0.00
20.77	13.96	94.48	15.34	126.94	2.28	116.24	4.43	48.53	14.75	0.89	0.00
21.98	14.44	95.70	14.90	126.97	2.20	115.45	4.78	47.30	14.56	0.81	−0.01
23.20	14.92	96.93	14.46	127.00	2.13	114.67	5.12	46.07	14.35	0.73	0.00
24.44	15.38	98.16	14.01	127.03	2.05	113.89	5.46	44.83	14.12	0.66	0.00
25.68	15.83	99.38	13.56	127.05	1.98	113.11	5.79	43.60	13.88	0.58	0.02
26.93	16.27	100.61	13.11	127.07	1.90	112.11	6.20	42.37	13.62	0.51	0.04

(Continued)

Table A1 Blade coordinates, mm (Fig. 2) (continued)

ξ	η	ξ	η	ξ	η	ξ	η	ξ	η	ξ	η
28.17	16.70	101.84	12.67	127.09	1.82	111.11	6.60	41.14	13.36	0.43	0.07
29.41	17.11	103.06	12.23	127.11	1.67	110.10	6.99	39.90	13.08	0.35	0.10
30.66	17.51	104.28	11.79	127.12	1.48	109.10	7.36	38.68	12.79	0.29	0.13
31.93	17.91	105.51	11.35	127.11	1.29	108.10	7.72	37.45	12.50	0.20	0.21
33.21	18.29	106.73	10.91	127.08	1.14	107.09	8.06	36.23	12.19	0.13	0.29
34.48	18.67	107.96	10.47	127.05	1.06	105.86	8.48	35.00	11.88	0.08	0.36
35.76	19.03	108.97	10.10	127.00	0.99	104.63	8.87	33.78	11.56	0.04	0.44
37.03	19.37	109.99	9.72	126.99	0.91	103.40	9.25	32.55	11.23	0.01	0.52
38.31	19.70	111.01	9.35	126.95	0.83	102.17	9.62	31.33	10.89	−0.01	0.59
39.61	20.03	112.03	8.97	126.90	0.76	100.94	9.99	30.11	10.54	−0.01	0.67
40.92	20.34	113.04	8.59	126.84	0.68	99.70	10.34	28.88	10.19	−0.02	0.74

Acknowledgments

This work was sponsoredby the Naval Air Warfare Center (Patuxent River), as part of a Fan and Compressor Stall Project. Stoney McAdams was Technical Monitor for the project, and his support is greatly appreciated.

References

[1]Johnsen, I. A., and Bullock, R. O. (eds.), "Aerodynamic Design of Axial-Flow Compressors," NASA SP-36, 1965.

[2]Gelder, T. F., Schmidt, J. F., Suder, K. L., and Hathaway M. D., "Design and Performance of Controlled-Diffusion Stator Compared with Original Double-Circular-Arc Stator," NASA TP 2852, 1989.

[3]Strazisar, A. J., Wood, J. R., Hathaway, M. D., and Suder, K. L., "Laser Anemometer Measurements in a Transonic Axial Flow Fan Rotor," NASA TP-2879, Nov. 1989.

[4]Rhoden, H. G., "Effect of Reynolds Number on the Flow of Air through a Cascade of Compressor Blades," Aeronautical Research Council, R&M 2919, 1956.

[5]Horlock, J. H., Shaw, R., Pollard, D., and Lewkowicz, A., "Reynolds Number Effects in Cascades and Axial Flow Compressors," *Journal of Engineering for Power*, Series A, 1964.

[6]Schlichting, H., and Das, A., "On the Influence of Turbulence Level on the Aerodynamic Losses of Axial Turbomachines," *Flow Research on Blading*, edited by L. S. Dzung, Elsevier, New York, 1970.

[7]Evans, B. J., "Effects of Free-Stream Turbulence on Blade Performance in a Compressor Cascade," Engineering Dept., Turbo/TR 26, Cambridge Univ., Cambridge, England, U.K., 1971.

[8]Roberts, W. B., "The Effect of Reynolds Number and Laminar Separation on Axial Cascade Performance," *Journal of Engineering for Power*, Series A, Vol. 97, No. 2, 1975, pp. 261–274.

[9]Sanger, N. L., "The Use of Optimization Techniques to Design Controlled-Diffusion Compressor Blading," NASA TM 82763, 1982; also American Society of Mechanical Engineers, Paper 82-GT-149, 1982.

[10]Elazar, Y., "A Mapping of the Viscous Flow Behavior in a Controlled-Diffusion Compressor Cascade Using Laser Doppler Velocimetry and Preliminary Evaluation of Codes for the Prediction of Stall," Ph.D. Dissertation, Dept. of Aeronautics and Astronautics, Naval Postgraduate School, Monterey, CA, 1988.

[11]Hobson, G. V., and Shreeve, R. P., "Inlet Turbulence Distortion and Viscous Flow Development in a Controlled-Diffusion Compressor Cascade at Very High Incidence," *Journal of Propulsion and Power*, Vol. 9, No. 3, 1993, pp. 397–404.

[12]Hansen, D. J., "Investigation of Second-Generation Controlled-Diffusion Compressor Blades in Cascade," M.S. Thesis, Aeronautical Engineering Dept., Naval Postgraduate School, Monterey, CA, 1995.

[13]Schnorenberg, D. G., "Investigation of the Effect of Reynolds Number on Laminar Separation Bubbles on Controlled-Diffusion Compressor Blades in Cascade," M.S. Thesis, Aeronautical Engineering Dept., Naval Postgraduate School, Monterey, CA, 1996.